

Article

Halogen Bonding Provides Heterooctameric Supramolecular Aggregation of Diaryliodonium Thiocyanate

Natalia S. Soldatova ¹, Vitalii V. Suslonov ¹, Troyana Yu. Kissler ¹, Daniil M. Ivanov ¹, Alexander S. Novikov ¹, Mekhman S. Yusubov ², Pavel S. Postnikov ^{2,3,*} and Vadim Yu. Kukushkin ^{1,4,*}

¹ Institute of Chemistry, Saint Petersburg State University, Saint Petersburg 199034, Russia; soldatovans@tpu.ru (N.S.S.); v.suslonov@spbu.ru (V.V.S.); troyanakissler@gmail.com (T.Y.K.); dan15101992@gmail.com (D.M.I.); a.s.novikov@spbu.ru (A.S.N.)

² Research School of Chemistry and Applied Biomedical Sciences, Tomsk Polytechnic University, Tomsk 634034, Russia; yusubov@mail.ru

³ Department of Solid State Engineering, Institute of Chemical Technology, 16628 Prague, Czech Republic

⁴ Laboratory of Crystal Engineering of Functional Materials, South Ural State University, 76, Lenin Av., Chelyabinsk 454080, Russia

* Correspondence: postnikov@tpu.ru (P.S.P.); v.kukushkin@spbu.ru (V.Y.K.)

Received: 6 March 2020; Accepted: 19 March 2020; Published: 22 March 2020



Abstract: The crystal structure of the newly synthesized 4-methoxyphenyl(phenyl)iodonium thiocyanate, [PhI(4-C₆H₄OMe)](SCN), represents the first example of 16-membered cyclic heterooctamer formed by halogen bonding between the iodonium cation and SCN[−]. Results of density functional theory (DFT) calculations followed by the topological analysis of the electron density distribution within the framework of the quantum theory of atoms in molecules (QTAIM) method at the ωB97XD/DZP-DKH level of theory reveal that energies of attractive intermolecular noncovalent interactions I⋯S and I⋯N (responsible for the formation of heterooctameric supramolecular clusters {PhI(4-C₆H₄OMe)}₄·{SCN}₄ in the solid state structure of [PhI(4-C₆H₄OMe)](SCN)) vary from 0.9 to 8.5 kcal/mol.

Keywords: halogen bonding; noncovalent interactions; DFT; QTAIM; hypervalent iodine; diaryliodonium salts; thiocyanate

1. Introduction

Halogen bonding (XB) has drawn increased attention in the past decade as a powerful tool for crystal engineering and supramolecular chemistry [1–5], drug design [6–8], organic synthesis [9–11], and as a route for facile tuning of physicochemical properties [12,13]. The geometry of XB interaction is conventionally studied by single-crystal X-ray diffraction (XRD) and, in accord with the International Union of Pure and Applied Chemistry (IUPAC) requirements [14], XB is confirmed when the R–X⋯Y contact value is less than the sum of their van der Waals radii and, in addition, ∠(R–X⋯Y) is close to 180°; the theoretical analysis of the electron density topology usually shows a bond path connecting X and Y and a bond critical point between X and Y.

The overwhelming majority of XB studies employing anionic species as XB acceptors explore halides (Cl[−], Br[−], I[−]) [15–17], while XB-accepting properties of pseudohalides are ill studied. In particular, our inspection of the Cambridge Structural Database (CSD) indicates a greater number of examples of R–X⋯S–C≡N–M XB in complexes featuring metal-bound SCN[−] and less than 20 structures including R–X⋯N≡C–S[−] or R–X⋯[−]S–C≡N XBs with uncomplexed SCN[−]. Bock and Hall [18–20] have identified XB between SCN[−] and iodine centers in tetraiodoethylene or tetraiodothiophene; SCN[−] in

these systems forms several XBs either via the thiocyanate N or S atoms to form the polymeric chains. Similar polymeric chains are formed between SCN^- and iodinated perfluoroarenes $\text{C}_6\text{I}_n\text{F}_{6-n}$ [21,22], CBr_4 [23,24], and other organic halides [25]. Organic monohalides also form XB in simple adducts that do not exhibit the polymeric motifs [26,27].

In general, the systems involving XB with SCN^- exhibit the following common features: $\angle(\text{X}\cdots\text{SCN})$ are close to 90° and $\angle(\text{X}\cdots\text{NCS})$ vary in the range from 115 to 170° . The XB-based polymeric structure incorporating SCN^- has also been observed in the hypervalent iodine(III) salt such as dibenziodolium thiocyanate [28]. Yet another example of XB between an iodonium cation and SCN^- featuring a heterotetrameric arrangement [29]. Geometrical parameters of XBs for hypervalent iodine(III) compounds agree with those described above ($\angle(\text{X}\cdots\text{SCN})$ and $\angle(\text{X}\cdots\text{NCS})$) for XB between monovalent organic halides and SCN^- .

Herein, we report on the hitherto unknown 16-membered heterooctameric cluster formed by XB between $[\text{PhI}(4\text{-C}_6\text{H}_4\text{OMe})]^+$ and SCN^- in iodonium salt **1** (Figure 1). Density functional theory (DFT) calculations approved the crucial contribution of $\text{C-I}\cdots\text{N}$ and $\text{C-I}\cdots\text{S}$ XBs in the formation of the heterooctamer cluster and also verified additional weak interactions as $\text{C}_2\text{-I}\cdots\text{S}$ XB and $\text{H}\cdots\text{S}$ hydrogen bonding (HB) (Figure 2). Our processing of the CCDC database allowed the identification of three relative heterooctamer clusters containing iodonium cation or SCN^- (Figure 3).

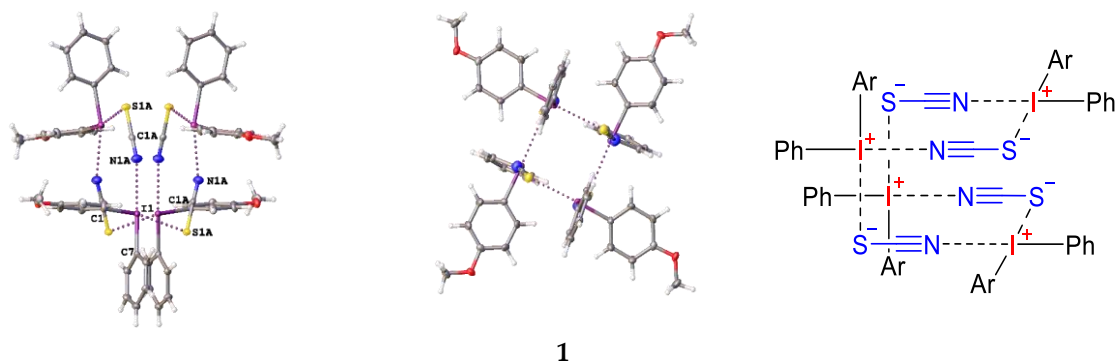


Figure 1. The $(\cdots\text{I}\cdots\text{SCN}\cdots)_4$ 16-membered halogen bonding (XB)-involving moiety in **1**.

2. Materials and Methods

2.1. Materials and Instrumentation

All reagents and solvents were obtained from commercial sources and used without further purification from freshly opened containers. Potassium thiocyanate was supplied by Reakhim (Moscow, Russia); methanol and acetone was supplied by Vekton (Saint Petersburg, Russia). $[\text{PhI}(4\text{-C}_6\text{H}_4\text{OMe})](\text{CF}_3\text{CO}_2)$ was prepared by the previously reported procedure [30]. The melting point was measured on a Stuart SMP30 apparatus (Cole-Parmer, Stone, Staffordshire, UK) in a capillary and is not corrected. High-resolution electrospray ionization (HRESI) mass-spectra were obtained on a Bruker maXis spectrometer (Bruker, Billerica, MA, USA) equipped with an ESI (Electrospray ionization) source. The instrument was operated in positive ion mode using an m/z range 50–1200. The nebulizer gas flow was 1.0 bar and the drying gas flow was 4.0 L/min. The NMR spectra were recorded on a Bruker Avance 400 (Bruker, Billerica, MA, USA) at ambient temperature; the residual solvent signal was used as the internal standard.

2.2. Computational Details

The single point calculations based on the experimental X-ray geometry of **1** were carried out at the DFT level of theory using the dispersion-corrected hybrid functional ωB97XD [31] with the help of the Gaussian-09 [32] program package (Gaussian, Inc., Wallingford, CT, USA). The Douglas–Kroll–Hess 2nd order scalar relativistic calculations requested relativistic core Hamiltonian were carried out using the

DZP-DKH basis sets [33–36] for all atoms. The topological analysis of the electron density distribution with the help of the atoms in molecules (QTAIM) method developed by Bader [37] has been performed by using the Multiwfn program (version 3.6) (Beijing Kein Research Center for Natural Sciences, Beijing, China) [38]. The Wiberg bond indices were computed by using the Natural Bond Orbital (NBO) partitioning scheme [39]. The Cartesian atomic coordinates for the model heterooctameric cluster $\{\text{PhI}(4\text{-C}_6\text{H}_4\text{OMe})\}_4\cdot\{\text{SCN}\}_4$ are presented in Table S1 (Supporting Information). The Hirshfeld molecular surfaces were generated by CrystalExplorer program (version 17.5) (The University of Western Australia, Perth, Australia) [40,41]. The normalized contact distances, d_{norm} [42], based on Bondi van der Waals radii [43], were mapped into the Hirshfeld surface. In the color scale, negative values of d_{norm} are visualized by the red color indicating contacts shorter than the sum of van der Waals radii. The white areas denote intermolecular distances close to van der Waals contacts with d_{norm} equal to zero. In turn, contacts longer than the sum of van der Waals radii with positive d_{norm} values are colored in blue.

2.3. Synthesis of $[\text{PhI}(4\text{-C}_6\text{H}_4\text{OMe})](\text{SCN})$ (**1**)

A solution of $[\text{PhI}(4\text{-C}_6\text{H}_4\text{OMe})(\text{CF}_3\text{CO}_2)]$ (1 mmol, 424 mg) in methanol (1 mL) was added dropwise to a solution of KSCN (5 mmol, 485 mg) in water (1 mL) at RT, whereupon the reaction mixture was stirred for 30 min, the precipitate formed was filtered off and washed with water (three 5-mL portions) at RT. The obtained 4-methoxyphenyl(phenyl)iodonium thiocyanate (**1**; 79%) was dried in air at RT. Compound **1** is a colorless crystalline solid; mp 132–134 °. ^1H NMR (400 MHz, $\text{DMSO-}d_6$), δ : 8.18 (m, 4H), 7.64 (t, $J = 7.6$ Hz, 1H), 7.51 (t, $J = 7.6$ Hz, 2H), 7.07 (d, $J = 8.8$ Hz, 2H), 3.79 (s, 3H). $^{13}\text{C}\{^1\text{H}\}$ NMR (100 MHz, $\text{DMSO-}d_6$), δ : 161.9, 137.2, 134.8, 131.8, 131.6, 129.5, 117.4, 117.3, 105.7, 55.7. HRESI⁺-MS: m/z calcd. for $\text{C}_{13}\text{H}_{12}\text{IO}^+$: 310.9927, found 310.9933.

2.4. Crystal Growth

Crystals of diaryliodonium thiocyanate **1** were grown by cocrystallization of the equimolar amounts of 4-methoxyphenyl(phenyl)iodonium trifluoroacetate [30] and potassium thiocyanate KSCN in acetone upon slow evaporation at 20–25 °C.

2.5. X-Ray Structure Determination

Suitable single-crystal of **1** was fixed on a micro mount, placed on an Xcalibur Eos diffractometer (Agilent Technologies, Yarnton, Oxfordshire, UK), and measured at 100(2) using monochromated $\text{Mo K}\alpha$ ($\lambda = 0.71073$) radiation. Using Olex2 (OlexSys Ltd, Durham, UK) [44], the structure was solved with the ShelXT (Shelx, Göttingen, Germany) [45] structure solution program using Intrinsic Phasing and refined with the ShelXL (Shelx, Göttingen, Germany) [45] refinement package using Least Squares minimization.

3. Results & Discussion

3.1. Crystal Structural Descriptions

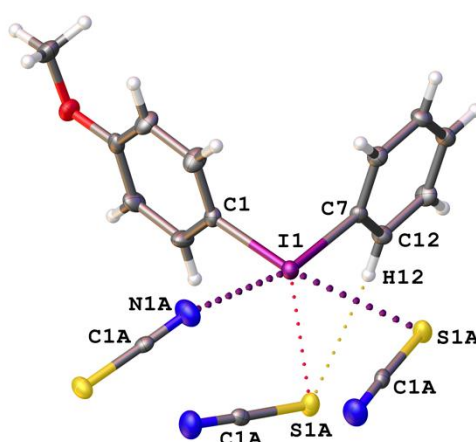
Iodonium salt **1** displays geometrical parameters that are typical for other diaryliodonium species, namely $\angle(\text{C1-I1-C7})$ 92.10(8)° is close to 90° and the I1–C1 and I1–C7 bonds are ~2.1 Å [46,47]. Upon our processing of CCDC, we found two more structures of diaryliodonium thiocyanates such as $[(\text{C}_6\text{H}_4)_2\text{I}](\text{SCN})$ [28] (**2**) and $[(\text{C}_6\text{F}_5)_2\text{I}](\text{SCN})$ [29] (**3**). If **2** exhibits a polymeric motif, **3** is a heterotetramer. The XB angles of **1** are similar to heterotetramer **3** and to those in other examples of XB involving monovalent halogen compounds: $\angle(\text{C1-I1}\cdots\text{S1A})$ 169.92(6)°; $\angle(\text{C1-I1}\cdots\text{N1A})$ 164.97(8)°; $\angle(\text{I1}\cdots\text{N1A}\equiv\text{C1A})$ 157.2(2)°; $\angle(\text{I1}\cdots\text{S1A-C1A})$ 89.66(8)° (Table 1). The noncovalent I1 \cdots S1A and I1 \cdots N1A distances are closer to the relevant values observed in polymeric **2**, rather than those in **3**; we assume that this is probably because of the electron withdrawing effect of C_6F_5 in **3**.

Table 1. Parameters of halogen bonding (XB) in **1**.

C–I...X	$d(\text{I}\cdots\text{X})$, Å	R_{IX}	$\angle(\text{C–I}\cdots\text{X})$, °	$\angle(\text{I}\cdots\text{X}\cdots\text{C})$, °	$E_{\text{int}}^{\text{a}}$	$E_{\text{int}}^{\text{b}}$
C7–I1...N1A	2.850(2)	0.81	164.97(8)	157.2(2)	8.5	8.4
C1–I1...S1A	3.1833(7)	0.84	169.92(6)	89.66(8)	6.0	5.9
C ₂ I1...S1A ^c	4.1531(7)	1.10	98.21(6) 86.33(6)	71.68(8)	0.9	1.3

^a $E_{\text{int}} = 0.68 (-V(\mathbf{r}))$, in kcal/mol (correlation developed exclusively for noncovalent interactions involving iodine atoms) [48]. ^b $E_{\text{int}} = 0.67 G(\mathbf{r})$, in kcal/mol (correlation developed exclusively for noncovalent interactions involving iodine atoms) [48]. ^c Theoretical calculations that are based on the experimentally determined atomic coordinates allow the determination of the bond critical point between these two atoms, see Section 3.4.

According to our theoretical calculations (Section 3.4), the $[\text{PhI}(4\text{-C}_6\text{H}_4\text{OMe})]^+$ cation noncovalently interacts with three thiocyanate anions (Figure 2) to form typical C1–I1...S1A and C7–I1...N1A XBs with two SCN^- and two weak I1...S1A and H12...S1A contacts with the third SCN^- .

**Figure 2.** Noncovalent interactions around $[\text{PhI}(4\text{-C}_6\text{H}_4\text{OMe})]^+$.

The H12...S1A interaction is hydrogen bonding [49] in view of the observed geometrical parameters, viz. $d(\text{H12}\cdots\text{S1A})$ 2.976 Å is slightly less than the vdW sum (3.00 Å), $\angle(\text{C12–H12}\cdots\text{S1A})$ 163.6°, $d(\text{C12}\cdots\text{S1A})$ 3.897(2) Å). The C₂I1...S1A interaction (Table 1) may be an XB according to the IUPAC definition [14], despite the unusual geometric parameters ($d(\text{C}_2\text{I}\cdots\text{S1A})$ 4.1531(7) Å is larger than the sum of Bondi vdW radii [50] ($R_{\text{vdW}}(\text{S}) + R_{\text{vdW}}(\text{I}) = 3.78$ Å); $\angle(\text{C1–I1}\cdots\text{S1A})$ and $\angle(\text{C7–I1}\cdots\text{S1A})$ are close to 90°). Resnati et al. [51] have performed electrostatic surface potential calculations for $[\text{Ph}_2\text{I}]^+$ and found four local potential maxima. Two out of four are opposite to the C–I covalent bonds and they were identified as σ -holes. The remaining two are under and above the C–I–C plane; these maxima were not attributed, however they can probably be treated as π -holes. One of these π -holes could be involved in weak I1...S1A interaction, which is perpendicular to the same C–I–C plane in the similar $[\text{PhI}(4\text{-C}_6\text{H}_4\text{OMe})]^+$ cation studied in this work.

3.2. Relevant Structures with Heterooctameric Motif

Only one example, $[(4\text{-MeC}_6\text{H}_4)_2\text{I}]\text{Br}$ [52] (Figure 3, CSD code: FASMUH), of the heterooctameric clusters stabilized by eight XBs between four iodonium cations and their counterions has been reported before our experiments. In this structure, similar to **1**, each diaryliodonium cation forms two XBs with counterions, which, however, are Br^- . In addition, $\{(4\text{-MeC}_6\text{H}_4)_2\text{I}\}_4\cdot\{\text{Br}\}_4$ is in another conformation comparing with $\{\text{PhI}(4\text{-C}_6\text{H}_4\text{OMe})\}_4\cdot\{\text{SCN}\}_4$ in **1**.

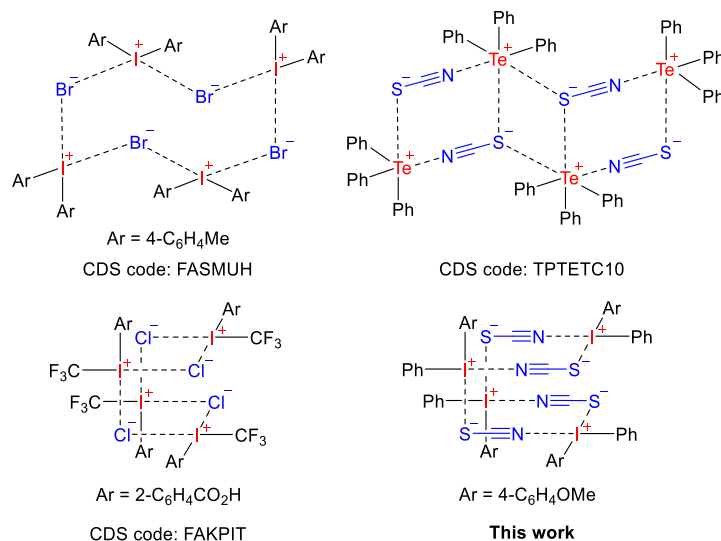


Figure 3. Relevant reported heterooctameric clusters (CSD codes: FASMUH, TPTETC10) and another one found upon our processing of the Cambridge Structural Database (CSD) (CSD code: FAKPIT).

The thiocyanate-based heterooctameric arrangement has been identified for [Te^{IV}Ph₃](SCN) (Figure 3; CSD code: TPTETC10). Its XRD structure displays three annulated cycles [53] and the conformation of {Te^{IV}Ph₃}₄·{SCN}₄ is the same as for {(4-MeC₆H₄)₂I}₄·{Br}₄ in the structure of FASMUH.

Our CCDC search verified another structure (Figure 3; CSD code: FAKPIT), which also demonstrates the heterooctameric aggregation of iodonium cations with their counter-ions, forming {CF₃I(2-C₆H₄CO₂H)}₄·{Cl}₄; in [54], the aggregation of [CF₃I(2-C₆H₄CO₂H)]Cl was not discussed. Notable that the heterooctamer in FAKPIT demonstrates the same conformation as {PhI(4-C₆H₄OMe)}₄·{SCN}₄ in **1**.

3.3. Hirshfeld Surface Analysis for the X-Ray Structure of **1**

The Hirshfeld surface (visualization of short interatomic contacts using sums of appropriate vdW radii) represents an area where molecules or atoms come into contact, and its analysis gives the possibility of additional insight into the nature of intermolecular interactions in the crystal state. We carried out the Hirshfeld surface analysis for the X-ray structure of **1** to understand what kind of intermolecular contacts give the largest contributions in the crystal packing. Figure 4 depicts the Hirshfeld surfaces for the [PhI(4-C₆H₄OMe)]⁺ and SCN[−] ions (mapping of the normalized contact distance d_{norm} was used for the visualization). In these surfaces, the regions of shortest intermolecular contacts are visualized by red circle areas. The main partial contributions of different intermolecular contacts to the Hirshfeld surfaces for the [PhI(4-C₆H₄OMe)]⁺ and SCN[−] ions are given in Table 2. The Hirshfeld surface analysis reveals that the crystal packing is determined primarily by intermolecular contacts involving H atoms. The parameters of morphology proper mean particles shape and appropriate surfaces and provide the basis for the optimal habit for the crystal. These parameters are useful for understanding the rheological attributes of the crystalline materials. The shape index (S) and curvedness (C) topological techniques [41] were employed for Hirshfeld surfaces of [PhI(4-C₆H₄OMe)]⁺ and SCN[−] ions in the crystal structure of **1**. The technique S provides the local shape of the 3D surface and define local topography (hollows and bumps in the 3D surface). The technique C represents the total curvature on the 3D surface and its mapping consists of a flat green region separated by dark blue edges. Figure 5 shows the shape index surfaces and curvedness index surfaces plotted over the Hirshfeld surfaces of [PhI(4-C₆H₄OMe)]⁺ and SCN[−] ions in the crystal structure of **1**. Taking into account that the Hirshfeld analysis does not allow the determination of energies of all these contacts, we conducted the appropriate DFT calculations.

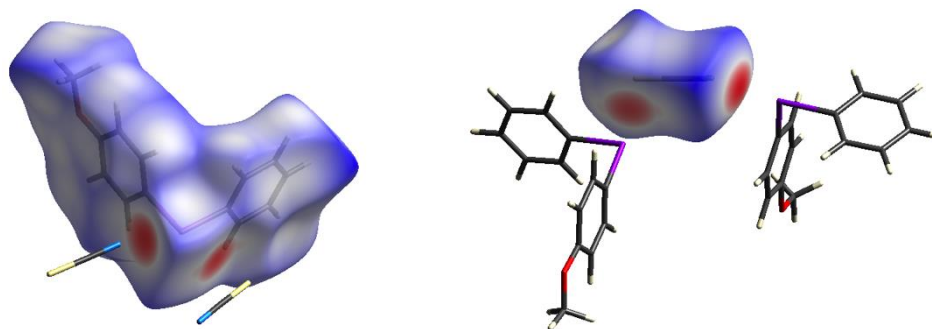


Figure 4. Hirshfeld surfaces for the $[\text{PhI}(4\text{-C}_6\text{H}_4\text{OMe})]^+$ (left) and SCN^- (right) ions.

Table 2. Main partial contributions of different intermolecular contacts to the Hirshfeld surfaces for the $[\text{PhI}(4\text{-C}_6\text{H}_4\text{OMe})]^+$ and SCN^- ions.

Moiety	Contributions of Different Intermolecular Contacts to the Molecular Hirshfeld Surface
{PhI(4-C ₆ H ₄ OMe)}	H...H 39.9%, C...H 27.0%, O...H 5.8%, S...H 5.5%, N...H 4.0%, I...N 3.5%, C...C 2.9%, I...C 2.7%, O...C 2.4%, I...H 2.4%, I...S 2.0%, N...C 1.1%, S...C 0.8%
{SCN}	S...H 37.1%, N...H 16.4%, C...H 13.5%, I...N 7.6%, I...C 7.0%, I...S 6.1%, N...N 5.6%, N...C 3.8%, S...C 2.8%

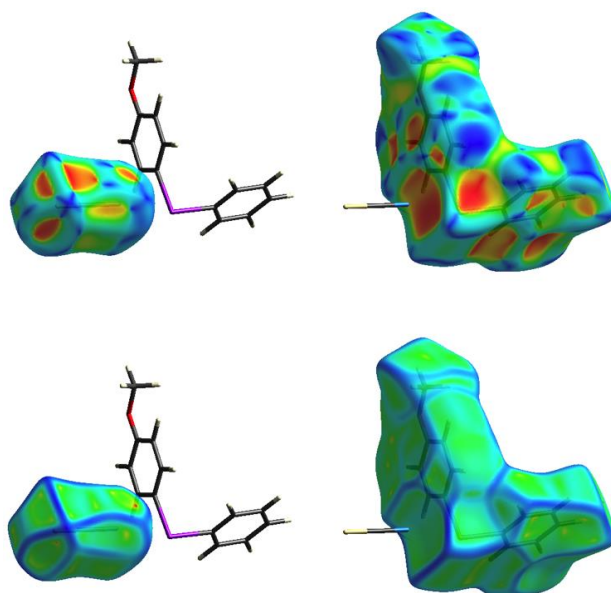


Figure 5. Shape index surfaces (top, color code: hollow—red; bumps—blue) and curvedness index surfaces (bottom, color code: edges—blue; flat regions—green) plotted over the Hirshfeld surfaces of $[\text{PhI}(4\text{-C}_6\text{H}_4\text{OMe})]^+$ and SCN^- ions in the crystal structure of **1**.

3.4. Theoretical Study of XB

Inspection of the crystallographic data reveals the presence of intermolecular noncovalent interactions I...S and I...N. These weak contacts are responsible for the supramolecular aggregation to furnish the heterooctameric clusters $\{\text{PhI}(4\text{-C}_6\text{H}_4\text{OMe})\}_4 \cdot \{\text{SCN}\}_4$. To confirm or disprove the hypothesis on the existence of these noncovalent interactions and to quantify their energies from a theoretical viewpoint, we carried out DFT calculations at the $\omega\text{B97XD}/\text{DZP-DKH}$ level of theory and topological analysis of the electron density distribution within the framework of Bader's theory (QTAIM method) [55] for the model system (Table 3 and Table S1, Supporting Information). The contour line diagrams of the Laplacian of electron density distribution $\nabla^2\rho(\mathbf{r})$, bond paths, and selected zero-flux surfaces for the

intermolecular noncovalent interactions I...S and I...N providing the heterooctameric supramolecular clusters $\{\text{PhI}(4\text{-C}_6\text{H}_4\text{OMe})\}_4\cdot\{\text{SCN}\}_4$ are shown in Figures 6–9. The visualization of these intermolecular contacts using noncovalent interaction (NCI) analysis based on promolecular electron density [56] (high quality grid, ~1,728,000 points in total) is shown in Figure 10.

Table 3. Values of the density of all electrons— $\rho(\mathbf{r})$, Laplacian of electron density— $\nabla^2\rho(\mathbf{r})$ and appropriate λ_2 eigenvalues (with promolecular approximation), energy density— H_b , potential energy density— $V(\mathbf{r})$, and Lagrangian kinetic energy— $G(\mathbf{r})$ (a.u.) at the bond critical points, corresponding to intermolecular noncovalent interactions I...S, H...S and I...N responsible for the formation of heterooctameric supramolecular associates $\{\text{PhI}(4\text{-C}_6\text{H}_4\text{OMe})\}_4\cdot\{\text{SCN}\}_4$, bond lengths— l (Å), Wiberg bond indices (WI), and estimated energies— E_{int} (kcal/mol) for these contacts.

Contact *	$\rho(\mathbf{r})$	$\nabla^2\rho(\mathbf{r})$	λ_2	H_b	$V(\mathbf{r})$	$G(\mathbf{r})$	l^{**}	WI	E_{int}^a	E_{int}^b
I1...N29	0.025	0.076	−0.028	0.000	−0.020	0.020	2.850	0.04	8.5	8.4
I1...S118	0.023	0.053	−0.022	0.000	−0.014	0.014	3.183	0.07	6.0	5.9
I1...S58	0.004	0.015	−0.005	0.001	−0.002	0.003	4.153	0.00	0.9	1.3
H8...S58	0.007	0.018	−0.009	0.001	−0.003	0.004	2.976	0.00	0.9	1.1

* Numeration of atoms in the model structure corresponds to their ordering in Table S1, Supporting Information.

** The shortest van der Waals radii for I, S, N and H atoms are 1.98, 1.80, 1.55 and 1.20 Å, respectively [43]. ^a $E_{\text{int}} = 0.68$ ($-V(\mathbf{r})$) (correlation developed exclusively for noncovalent interactions involving iodine atoms) [48]. ^b $E_{\text{int}} = 0.67$ ($G(\mathbf{r})$) (correlation developed exclusively for noncovalent interactions involving iodine atoms) [48].

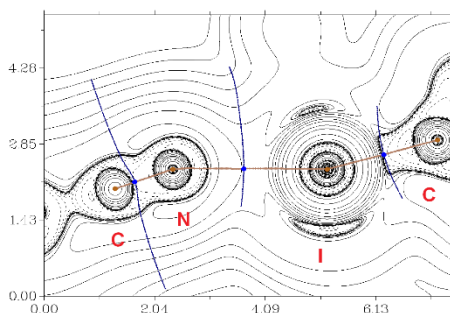


Figure 6. Contour line diagram of the Laplacian of electron density distribution $\nabla^2\rho(\mathbf{r})$, bond paths and selected zero-flux surfaces referring to intermolecular noncovalent interactions I1...N29 in the model heterooctameric cluster $\{\text{PhI}(4\text{-C}_6\text{H}_4\text{OMe})\}_4\cdot\{\text{SCN}\}_4$. Bond critical points are shown in blue, nuclear critical points—in pale brown, length units on X and Y axis are given in Å. Numeration of atoms in the model structure corresponds to their ordering in Table S1, Supporting Information.

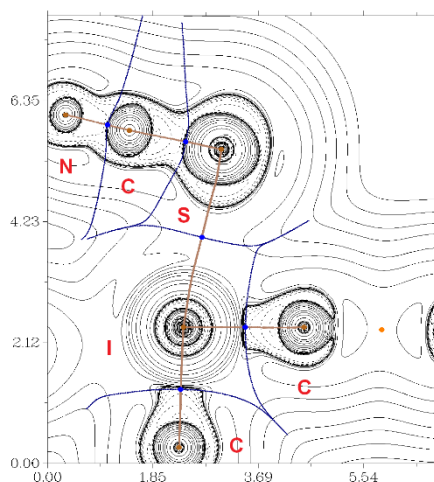


Figure 7. Contour line diagram of the Laplacian of electron density distribution $\nabla^2\rho(\mathbf{r})$, bond paths and selected zero-flux surfaces referring to intermolecular noncovalent interactions I1...S118 in the model heterooctameric cluster $\{\text{PhI}(4\text{-C}_6\text{H}_4\text{OMe})\}_4\cdot\{\text{SCN}\}_4$. The remaining figure legend is in Figure 6.

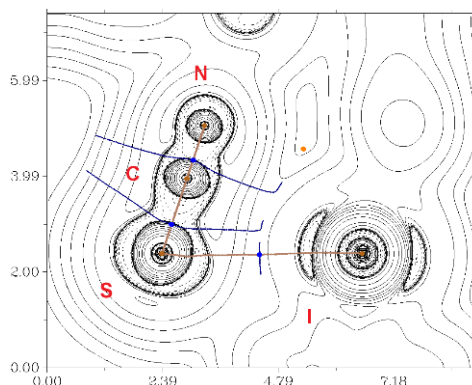


Figure 8. Contour line diagram of the Laplacian of electron density distribution $\nabla^2\rho(\mathbf{r})$, bond paths and selected zero-flux surfaces referring to intermolecular noncovalent interactions I1...S58 in the model heterooctameric cluster $\{\text{PhI}(4\text{-C}_6\text{H}_4\text{OMe})\}_4\cdot\{\text{SCN}\}_4$. The remaining figure legend is in Figure 6.

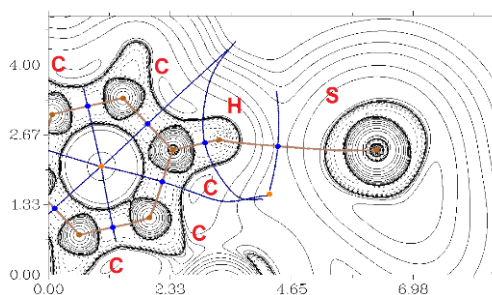


Figure 9. Contour line diagram of the Laplacian of electron density distribution $\nabla^2\rho(\mathbf{r})$, bond paths and selected zero-flux surfaces referring to hydrogen bond C7–H8...S58 in model heterooctameric cluster $\{\text{PhI}(4\text{-C}_6\text{H}_4\text{OMe})\}_4\cdot\{\text{SCN}\}_4$. The remaining figure legend is in Figure 6.

The quantum theory of atoms in molecules (QTAIM) analysis demonstrates the presence of appropriate bond critical points (BCPs) for intermolecular noncovalent interactions I...S and I...N in the heterooctameric clusters $\{\text{PhI}(4\text{-C}_6\text{H}_4\text{OMe})\}_4\cdot\{\text{SCN}\}_4$ (the Poincaré–Hopf relationship was satisfied during the QTAIM analysis of the model system and all critical points were found). The low magnitude of the electron density (0.004–0.025 a.u.), positive values of the Laplacian of electron density (0.015–0.076 a.u.), and zero or very close to zero positive energy density (0.000–0.001 a.u.) in these BCPs are typical for such weak contacts [57–61]. The estimated energies for these noncovalent interactions according to the correlations proposed by Tsirelson et al. [48] are 0.9–1.3 kcal/mol (long I...S contacts), 5.9–6.0 kcal/mol (short I...S contacts), and 8.4–8.5 kcal/mol (I...N contacts). The balance between the Lagrangian kinetic energy $G(\mathbf{r})$ and potential energy density $V(\mathbf{r})$ at the bond critical points reveals the nature of these interactions, if the ratio $-G(\mathbf{r})/V(\mathbf{r}) > 1$ is satisfied, then the nature of appropriate interaction is purely noncovalent, in the case of $-G(\mathbf{r})/V(\mathbf{r}) < 1$ some covalent component takes place [62]; based on this criterion, one can state that a covalent contribution in I...S and I...N interactions is negligible; this correlates with the small values of the Wiberg bond indices for these contacts (0.00–0.07). The Laplacian of electron density in BCPs is typically decomposed into the sum of contributions along the three principal axes of maximal variation, giving the three eigenvalues of the Hessian matrix (λ_1 , λ_2 , and λ_3), and the sign of λ_2 can be utilized to distinguish bonding (attractive, $\lambda_2 < 0$) weak interactions from nonbonding ones (repulsive, $\lambda_2 > 0$) [56,63]. Thus, the sign of λ_2 in the appropriate BCPs for the I...S and I...N contacts in $\{\text{PhI}(4\text{-C}_6\text{H}_4\text{OMe})\}_4\cdot\{\text{SCN}\}_4$ reveals that these contacts are of an attractive nature.

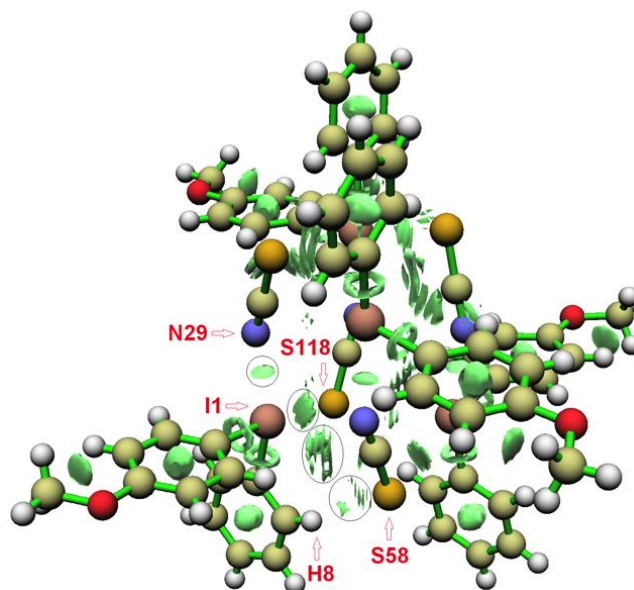


Figure 10. Visualization of intermolecular contacts I...S and I...N in $\{\text{PhI}(4\text{-C}_6\text{H}_4\text{OMe})\}_4\cdot\{\text{SCN}\}_4$ using noncovalent interaction (NCI) analysis based on promolecular electron density (high quality grid, ~1,728,000 points in total). Numeration of atoms in the model structure corresponds to their ordering in Table S1, Supporting Information.

4. Conclusions

We found that XBs between the iodonium cations and thiocyanate anions could provide not only the polymeric or heterotetrameric motifs, but also add complexity to the 16-membered heterooctameric clusters $\{\text{PhI}(4\text{-C}_6\text{H}_4\text{OMe})\}_4\cdot\{\text{SCN}\}_4$. DFT calculations verified three XBs between I and SCN^- , namely two conventional contacts with σ -holes of I ($\text{C}-\text{I}\cdots\text{S}$ and $\text{C}-\text{I}\cdots\text{N}$), and one contact with possible iodine π -hole ($\text{C}_2-\text{I}\cdots\text{S}$). Three relative heterooctameric structures were found by our processing of CCDC. Despite the limited number of the relevant heterooctameric clusters, the similar conformation of two iodonium salt clusters allows the presumption that heterooctamers can be more spread structural motifs.

Supplementary Materials: The following are available online at <http://www.mdpi.com/2073-4352/10/3/230/s1>, Table S1: Cartesian atomic coordinates for model heterooctameric cluster $\{\text{PhI}(p\text{-(MeO)C}_6\text{H}_4)\}_4\cdot\{\text{SCN}\}_4$, Table S2: Crystal data and structure refinement for **1**; NMR spectra of **1**.

Author Contributions: Conceptualization, N.S.S., D.M.I., M.S.Y., P.S.P. and V.Y.K.; methodology, N.S.S. and D.M.I.; validation, D.M.I., M.S.Y., P.S.P. and V.Y.K.; formal analysis, N.S.S., D.M.I. and A.S.N.; investigation, N.S.S., V.V.S., T.Y.K., D.M.I. and A.S.N.; resources, D.M.I., M.S.Y., P.S.P. and V.Y.K.; data curation, D.M.I. and A.S.N.; writing—original draft preparation, N.S.S., D.M.I. and A.S.N.; writing—review and editing, D.M.I., P.S.P. and V.Y.K.; visualization, N.S.S., D.M.I. and A.S.N.; supervision, D.M.I.; project administration, D.M.I.; funding acquisition, N.S.S. All authors have read and agreed to the published version of the manuscript.

Funding: This work was funded by Russian Science Foundation, grant number 19-73-00007.

Acknowledgments: Authors are grateful the Center for X-ray Diffraction Studies, Magnetic Resonance Research Center, and Center for Chemical Analysis and Materials Research (all belonging to Saint Petersburg State University) for the physicochemical studies. V.Y.K. thanks South Ural State University (Act 211 Government of the Russian Federation, contract No 02.A03.21.0011) for putting facilities at the author's disposal.

Conflicts of Interest: The authors declare no conflict of interest.

References

1. Berger, G.; Soubhye, J.; Meyer, F. Halogen bonding in polymer science: From crystal engineering to functional supramolecular polymers and materials. *Polym. Chem.* **2015**, *6*, 3559–3580. [[CrossRef](#)]
2. Gilday, L.C.; Robinson, S.W.; Barendt, T.A.; Langton, M.J.; Mullaney, B.R.; Beer, P.D. Halogen Bonding in Supramolecular Chemistry. *Chem. Rev.* **2015**, *115*, 7118–7195. [[CrossRef](#)] [[PubMed](#)]

3. Meazza, L.; Foster, J.A.; Fucke, K.; Metrangolo, P.; Resnati, G.; Steed, J.W. Halogen-bonding-triggered supramolecular gel formation. *Nat. Chem.* **2013**, *5*, 42–47. [[CrossRef](#)] [[PubMed](#)]
4. Bertani, R.; Sgarbossa, P.; Venzo, A.; Lej, F.; Amati, M.; Resnati, G.; Pilati, T.; Metrangolo, P.; Terraneo, G. Halogen bonding in metal-organic-supramolecular networks. *Coord. Chem. Rev.* **2010**, *254*, 677–695. [[CrossRef](#)]
5. Sinnwell, M.A.; Blad, J.N.; Thomas, L.R.; MacGillivray, L.R. Structural flexibility of halogen bonds showed in a single-crystal-to-single-crystal [2+2] photodimerization. *IUCr* **2018**, *5*, 491–496. [[CrossRef](#)]
6. Ibrahim, M.A.A. Molecular mechanical study of halogen bonding in drug discovery. *J. Comput. Chem.* **2011**, *32*, 2564–2574. [[CrossRef](#)]
7. Scholfield, M.R.; Zanden, C.M.V.; Carter, M.; Ho, P.S. Halogen bonding (X-bonding): A biological perspective. *Protein Sci.* **2013**, *22*, 139–152. [[CrossRef](#)]
8. Danelius, E.; Andersson, H.; Jarvoll, P.; Lood, K.; Gräfenstein, J.; Erdélyi, M. Halogen Bonding: A Powerful Tool for Modulation of Peptide Conformation. *Biochemistry* **2017**, *56*, 3265–3272. [[CrossRef](#)]
9. Sutar, R.L.; Huber, S.M. Catalysis of Organic Reactions through Halogen Bonding. *ACS Catal.* **2019**, *9*, 9622–9639. [[CrossRef](#)]
10. Bulfield, D.; Huber, S.M. Halogen Bonding in Organic Synthesis and Organocatalysis. *Chem. A Eur. J.* **2016**, *22*, 14434–14450. [[CrossRef](#)]
11. Kinzhalov, M.A.; Kashina, M.V.; Mikherdov, A.S.; Mozheeva, E.A.; Novikov, A.S.; Smirnov, A.S.; Ivanov, D.M.; Kryukova, M.A.; Ivanov, A.Y.; Smirnov, S.N.; et al. Dramatically Enhanced Solubility of Halide-Containing Organometallic Species in Diiodomethane: The Role of Solvent···Complex Halogen Bonding. *Angew. Chem. Int. Ed.* **2018**, *57*, 12785–12789. [[CrossRef](#)] [[PubMed](#)]
12. Landenberger, K.B.; Bolton, O.; Matzger, A.J. Energetic–Energetic Cocrystals of Diacetone Diperoxide (DADP): Dramatic and Divergent Sensitivity Modifications via Cocrystallization. *J. Am. Chem. Soc.* **2015**, *137*, 5074–5079. [[CrossRef](#)] [[PubMed](#)]
13. Sivchik, V.V.; Solomatina, A.I.; Chen, Y.-T.; Karttunen, A.J.; Tunik, S.P.; Chou, P.-T.; Koshevoy, I.O. Halogen Bonding to Amplify Luminescence: A Case Study Using a Platinum Cyclometalated Complex. *Angew. Chem. Int. Ed.* **2015**, *54*, 14057–14060. [[CrossRef](#)] [[PubMed](#)]
14. Desiraju, G.R.; Ho, P.S.; Kloo, L.; Legon, A.C.; Marquardt, R.; Metrangolo, P.; Politzer, P.; Resnati, G.; Rissanen, K. Definition of the halogen bond (IUPAC Recommendations 2013). *Pure Appl. Chem.* **2013**, *85*, 1711–1713. [[CrossRef](#)]
15. Ivanov, D.M.; Kinzhalov, M.A.; Novikov, A.S.; Ananyev, I.V.; Romanova, A.A.; Boyarskiy, V.P.; Haukka, M.; Kukushkin, V.Y. H₂C(X)–X···X– (X = Cl, Br) Halogen Bonding of Dihalomethanes. *Cryst. Growth Des.* **2017**, *17*, 1353–1362. [[CrossRef](#)]
16. Sarwar, M.G.; Dragisic, B.; Sagoo, S.; Taylor, M.S. A Tridentate Halogen-Bonding Receptor for Tight Binding of Halide Anions. *Angew. Chem. Int. Ed.* **2010**, *49*, 1674–1677. [[CrossRef](#)]
17. Caballero, A.; Zapata, F.; White, N.G.; Costa, P.J.; Félix, V.; Beer, P.D. A Halogen-Bonding Catenane for Anion Recognition and Sensing. *Angew. Chem. Int. Ed.* **2012**, *51*, 1876–1880. [[CrossRef](#)]
18. Bock, H.; Holl, S. Wechselwirkungen in molekülkristallen, 179 [1, 2]. σ -donator/akzeptor-komplexe {I₂C=Cl₂···X \ominus } (X \ominus = Cl \ominus , Br \ominus , I \ominus , SCN \ominus) von tetraiodethen in tetra(n-butyl)ammoniumhalogenid-salzen. *Z. Naturforsch. B* **2002**, *57*, 713–725. [[CrossRef](#)]
19. Bock, H.; Holl, S. Wechselwirkungen in Molekülkristallen, 180 [1, 2]. σ -Donator/Akzeptor-Komplexe {S(Cl)₄···X \ominus } (X \ominus = I \ominus , SCN \ominus) von Tetraiodthiophen in Tetra(n-butyl)ammoniumhalogenid-Salzen/Interaction in Molecular Crystals, 180 [1, 2]. -Donor/Acceptor Complexes {S(Cl)₄}. *Z. Naturforsch. B* **2002**, *57*, 835–842. [[CrossRef](#)]
20. Bock, H.; Holl, S. Wechselwirkungen in Molekülkristallen, 181 [1, 2]. σ -Donator/Akzeptor-Komplexe {MAI₄···X \ominus } (X \ominus = Br \ominus , I \ominus , SCN \ominus) der Tetraiod-Akzeptormoleküle MAI₄ (MA = Ethen, Thiophen, N-Methylpyrrol) in Tetraphenylphosphoniumhalogenid-Salzen Interaction in Molecula. *Z. Naturforsch. B* **2002**, *57*, 843–858.
21. Cauliez, P.; Polo, V.; Roisnel, T.; Llusar, R.; Fourmigué, M. The thiocyanate anion as a polydentate halogen bond acceptor. *CrystEngComm* **2010**, *12*, 558–566. [[CrossRef](#)]
22. Viger-Gravel, J.; Korobkov, I.; Bryce, D.L. Multinuclear Solid-State Magnetic Resonance and X-ray Diffraction Study of Some Thiocyanate and Selenocyanate Complexes Exhibiting Halogen Bonding. *Cryst. Growth Des.* **2011**, *11*, 4984–4995. [[CrossRef](#)]
23. Rosokha, S.V.; Stern, C.L.; Swartz, A.; Stewart, R. Halogen bonding of electrophilic bromocarbons with pseudohalide anions. *Phys. Chem. Chem. Phys.* **2014**, *16*, 12968–12979. [[CrossRef](#)] [[PubMed](#)]

24. Grounds, O.; Zeller, M.; Rosokha, S.V. Structural preferences in strong anion- π and halogen-bonded complexes: π - And σ -holes vs. frontier orbitals interaction. *New J. Chem.* **2018**, *42*, 10572–10583. [[CrossRef](#)]
25. Riel, A.M.S.; Jessop, M.J.; Decato, D.A.; Massena, C.J.; Nascimento, V.R.; Berryman, O.B. Experimental investigation of halogen-bond hard–soft acid–base complementarity. *Acta Crystallogr. Sect. B Struct. Sci. Cryst. Eng. Mater.* **2017**, *73*, 203–209. [[CrossRef](#)]
26. Pramanik, A.; Majumdar, S.; Das, G. Aryl azo imidazoles assisted assembly of anion/anion–water through salt formation. *CrystEngComm* **2010**, *12*, 250–259. [[CrossRef](#)]
27. Phonsri, W.; Harding, D.J.; Harding, P.; Murray, K.S.; Moubaraki, B.; Gass, I.A.; Cashion, J.D.; Jameson, G.N.L.; Adams, H. Stepped spin crossover in Fe(III) halogen substituted quinolyalsalicylaldimine complexes. *Dalt. Trans.* **2014**, *43*, 17509–17518. [[CrossRef](#)]
28. Postnikov, P.S.; Guselnikova, O.A.; Yusubov, M.S.; Yoshimura, A.; Nemykin, V.N.; Zhdankin, V.V. Preparation and X-ray structural study of dibenziodolium derivatives. *J. Org. Chem.* **2015**, *80*, 5783–5788. [[CrossRef](#)]
29. Hirschberg, M.E.; Barthen, P.; Frohn, H.J.; Bläser, D.; Tobey, B.; Jansen, G. Interaction of the electrophilic bis(pentafluorophenyl)iodonium cation [(C₆F₅)₂I]⁺ with the ambident pseudohalogenide anions [SCN]⁻ and [CN]⁻. *J. Fluor. Chem.* **2014**, *163*, 28–33. [[CrossRef](#)]
30. Soldatova, N.S.; Postnikov, P.S.; Yusubov, M.S.; Wirth, T. Flow Synthesis of Iodonium Trifluoroacetates through Direct Oxidation of Iodoarenes by Oxone®. *Eur. J. Org. Chem.* **2019**, *2019*, 2081–2088. [[CrossRef](#)]
31. Chai, J.D.; Head-Gordon, M. Long-range corrected hybrid density functionals with damped atom-atom dispersion corrections. *Phys. Chem. Chem. Phys.* **2008**, *10*, 6615–6620. [[CrossRef](#)] [[PubMed](#)]
32. Frisch, M.J.; Trucks, G.W.; Schlegel, H.B.; Scuseria, G.E.; Robb, M.A.; Cheeseman, J.R.; Scalmani, G.; Barone, V.; Mennucci, B.; Petersson, G.A.; et al. *Gaussian 09, Revision C.01*; Gaussian, Inc.: Wallingford CT, UK, 2010.
33. Barros, C.L.; de Oliveira, P.J.P.; Jorge, F.E.; Canal Neto, A.; Campos, M. Gaussian basis set of double zeta quality for atoms Rb through Xe: Application in non-relativistic and relativistic calculations of atomic and molecular properties. *Mol. Phys.* **2010**, *108*, 1965–1972. [[CrossRef](#)]
34. Canal Neto, A.; Jorge, F.E. All-electron double zeta basis sets for the most fifth-row atoms: Application in DFT spectroscopic constant calculations. *Chem. Phys. Lett.* **2013**, *582*, 158–162. [[CrossRef](#)]
35. de Berrêdo, R.C.; Jorge, F.E. All-electron double zeta basis sets for platinum: Estimating scalar relativistic effects on platinum(II) anticancer drugs. *J. Mol. Struct. THEOCHEM* **2010**, *961*, 107–112. [[CrossRef](#)]
36. Jorge, F.E.; Canal Neto, A.; Camiletti, G.G.; MacHado, S.F. Contracted Gaussian basis sets for Douglas-Kroll-Hess calculations: Estimating scalar relativistic effects of some atomic and molecular properties. *J. Chem. Phys.* **2009**, *130*, 064108. [[CrossRef](#)]
37. Bader, R.F.W. A quantum theory of molecular structure and its applications. *Chem. Rev.* **1991**, *91*, 893–928. [[CrossRef](#)]
38. Lu, T.; Chen, F. Multiwfn: A multifunctional wavefunction analyzer. *J. Comput. Chem.* **2012**, *33*, 580–592. [[CrossRef](#)]
39. Glendening, E.D.; Landis, C.R.; Weinhold, F. Natural bond orbital methods. *WIREs Comput. Mol. Sci.* **2012**, *2*, 1–42. [[CrossRef](#)]
40. Turner, M.J.; McKinnon, J.J.; Wolff, S.K.; Grimwood, D.J.; Spackman, P.R.; Jayatilaka, D.; Spackman, M.A. *CrystalExplorer17*; University of Western Australia: Perth, Australia, 2017.
41. Spackman, M.A.; Jayatilaka, D. Hirshfeld surface analysis. *CrystEngComm* **2009**, *11*, 19–32. [[CrossRef](#)]
42. McKinnon, J.J.; Jayatilaka, D.; Spackman, M.A. Towards quantitative analysis of intermolecular interactions with Hirshfeld surfaces. *Chem. Commun.* **2007**, 3814–3816. [[CrossRef](#)]
43. Bondi, A. van der Waals Volumes and Radii of Metals in Covalent Compounds. *J. Phys. Chem.* **1966**, *70*, 3006–3007. [[CrossRef](#)]
44. Dolomanov, O.V.; Bourhis, L.J.; Gildea, R.J.; Howard, J.A.K.; Puschmann, H. OLEX2: A complete structure solution, refinement and analysis program. *J. Appl. Crystallogr.* **2009**, *42*, 339–341. [[CrossRef](#)]
45. Sheldrick, G.M. Crystal structure refinement with SHELXL. *Acta Crystallogr. Sect. C Struct. Chem.* **2015**, *71*, 3–8. [[CrossRef](#)] [[PubMed](#)]
46. Zhdankin, V.V. *Hypervalent Iodine Chemistry*; John Wiley & Sons Ltd: Chichester, UK, 2013; ISBN 9781118341155.
47. Yusubov, M.S.; Maskaev, A.V.; Zhdankin, V.V. Iodonium salts in organic synthesis. *Arkivoc* **2011**, *2011*, 370–409.
48. Bartashevich, E.V.; Tsirelson, V.G. Interplay between non-covalent interactions in complexes and crystals with halogen bonds. *Russ. Chem. Rev.* **2014**, *83*, 1181–1203. [[CrossRef](#)]

49. Arunan, E.; Desiraju, G.R.; Klein, R.A.; Sadlej, J.; Scheiner, S.; Alkorta, I.; Clary, D.C.; Crabtree, R.H.; Dannenberg, J.J.; Hobza, P.; et al. Definition of the hydrogen bond (IUPAC Recommendations 2011). *Pure Appl. Chem.* **2011**, *83*, 1637–1641. [[CrossRef](#)]
50. Bondi, A. van der Waals Volumes and Radii. *J. Phys. Chem.* **1964**, *68*, 441–451. [[CrossRef](#)]
51. Cavallo, G.; Murray, J.S.; Politzer, P.; Pilati, T.; Ursini, M.; Resnati, G. Halogen bonding in hypervalent iodine and bromine derivatives: Halonium salts. *IUCrJ* **2017**, *4*, 411–419. [[CrossRef](#)]
52. Alcock, N.W.; Countryman, R.M. Secondary bonding. Part 14. Structural isomerism in diaryliodonium halides and the structure of di(p-tolyl)iodonium bromide. *J. Chem. Soc. Dalt. Trans.* **1987**, 193–196. [[CrossRef](#)]
53. Lee, J.S.; Titus, D.D.; Ziolo, R.F. Structural Characterization of the Bioligomeric Triphenyltelluronium Thiocyanate Salt, $((C_6H_5)_3Te(NCS))_4((C_6H_5)_3Te(NCS))_2$. *Inorg. Chem.* **1977**, *16*, 2487–2492. [[CrossRef](#)]
54. Brantley, J.N.; Samant, A.V.; Toste, F.D. Isolation and reactivity of trifluoromethyl iodonium salts. *ACS Cent. Sci.* **2016**, *2*, 341–350. [[CrossRef](#)] [[PubMed](#)]
55. Bader, R.F.W. *Bader Atoms in Molecules: A Quantum Theory*; Oxford University Press, Clarendon Press: Oxford, UK, 1990; ISBN 9780198558651.
56. Johnson, E.R.; Keinan, S.; Mori-Saánchez, P.; Contreras-García, J.; Cohen, A.J.; Yang, W. Revealing Noncovalent Interactions. *J. Am. Chem. Soc.* **2010**, *132*, 6498–6506. [[CrossRef](#)] [[PubMed](#)]
57. Eliseeva, A.A.; Ivanov, D.M.; Novikov, A.S.; Rozhkov, A.V.; Korniyakov, I.V.; Dubovtsev, A.Y.; Kukushkin, V.Y. Hexaiododiplatinate(ii) as a useful supramolecular synthon for halogen bond involving crystal engineering. *Dalt. Trans.* **2020**, *49*, 356–367. [[CrossRef](#)] [[PubMed](#)]
58. Adonin, S.A.; Bondarenko, M.A.; Novikov, A.S.; Abramov, P.A.; Sokolov, M.N.; Fedin, V.P. Halogen bonding in the structures of pentaiodobenzoic acid and its salts. *CrystEngComm* **2019**, *21*, 6666–6670. [[CrossRef](#)]
59. Eliseeva, A.A.; Ivanov, D.M.; Novikov, A.S.; Kukushkin, V.Y. Recognition of the π -hole donor ability of iodopentafluorobenzene—a conventional σ -hole donor for crystal engineering involving halogen bonding. *CrystEngComm* **2019**, *21*, 616–628. [[CrossRef](#)]
60. Kryukova, M.; Sapegin, A.; Novikov, A.; Krasavin, M.; Ivanov, D. New Crystal Forms for Biologically Active Compounds. Part I: Noncovalent Interactions in Adducts of Nevirapine with XB Donors. *Crystals* **2019**, *9*, 71. [[CrossRef](#)]
61. Novikov, A.S.; Ivanov, D.M.; Bikbaeva, Z.M.; Bokach, N.A.; Kukushkin, V.Y. Noncovalent Interactions Involving Iodofluorobenzenes: The Interplay of Halogen Bonding and Weak $Ip(O)\cdots\pi$ -Hole Arene Interactions. *Cryst. Growth Des.* **2018**, *18*, 7641–7654. [[CrossRef](#)]
62. Espinosa, E.; Alkorta, I.; Elguero, J.; Molins, E. From weak to strong interactions: A comprehensive analysis of the topological and energetic properties of the electron density distribution involving $X-H\cdots F-Y$ systems. *J. Chem. Phys.* **2002**, *117*, 5529–5542. [[CrossRef](#)]
63. Contreras-García, J.; Johnson, E.R.; Keinan, S.; Chaudret, R.; Piquemal, J.-P.; Beratan, D.N.; Yang, W. NCIPLLOT: A Program for Plotting Noncovalent Interaction Regions. *J. Chem. Theory Comput.* **2011**, *7*, 625–632. [[CrossRef](#)]

